Korean J. Chem. Eng., 39(8), 2034-2043 (2022)
DOI: 10.1007/s11814-022-1162-8

pISSN: 0256-1115
eISSN: 1975-7220

Effects of opening design of gas distribution plate on fluidization of the synthesis process of organosilicon monomer

Weichuan Tan*, Shanlin Du*, Yunfei He, Guoqiang Lv*,†, Wenhui Ma*, Aimin Xing***, and Jie Huang*****

*Engineering Research Center for Silicon Metallurgy and Silicon Materials of Yunnan Provincial Universities,
Faculty of Metallurgical and Energy Engineering, Kunming University of Science and Technology, Kunming 650093, China
**Yunnan Energy Research Institute Co., Ltd., Kunming 650093, China
***Yunnan Energy Investment Silicon Material Technology Development Co., Ltd., Kunming 650093, China

(*Received 12 September 2021 • Revised 5 April 2022 • Accepted 28 April 2022*)

Abstract−The structure of the gas distributor was optimized to enhance the reaction rate of direct synthesis of silicone monomers in a fluidized bed. In this work, the opening rate range was selected by the critical pressure drop ratio, and the influences of opening ratio and the holes quantities of distribution plate on the synthesis process were systematically studied by numerical simulation approaches. The fluidization velocity was simplified by Reylows' and Archimedes' criterion numbers. To better predict the gas-solid fluidization characteristics in the bed, the drag model was modified by the critical fluidization velocity. In addition, the distributor performance was investigated from the perspectives of solid phase volume fraction, pressure drop change, bubble behavior and power spectrum analysis, etc. The results show that the distribution plate pressure drop ratio is about 0.11679 at the opening rate of 0.53%, which meets the design criterion of reducing the dissipation while increasing the fluidized quality. A high frequency and a low amplitude arise at the opening rate of 0.53%, indicating the corresponding favorable efficiency of heat and mass transfer. The maximum fluctuation range of the solid phase distribution with Φ=0.53% is only 1.7%, indicating that the inhomogeneity of the solid phase fraction distribution is the lowest, and the fluidization stability is improved by about 30%. Consequently, Φ=0.53% is proposed as the best distributor configuration and enhanced the monomer synthesis efficiency.

Keywords: Fluidized Bed Reactor, Distribution Plate, Perforated Ratio, Two-fluid Model, Drag Model, Direct Synthesis

INTRODUCTION

With the development and progress of the organic silicone industry in the past 25 years, organic silicones have become indispensable supporting materials for nationally-strategic emerging industries. Organic silicone has a unique molecular structure due to the dual properties of inorganic structures and organic groups endows it with a unique molecular structure [1], which makes the development and utilization of downstream silicone products very promising. Additionally, the supply of upstream silicone monomers is required for the growth and improvement of downstream products comprehensively and systematically. At present, the direct method is still needed for the industrial production process of organosilicon monomers, and its mechanism has been fully described in the literature [2-5]. In the process of organosilicon synthesis, the following conditions are achieved: the silicon powder, catalyst and co-catalyst need to be evenly mixed; the temperature is required to reach about 300 °C in the treating process of activation to form the active centers of Si-Cu, and methylchlorosilane (MC) gas is formed by reacting with the CH_3Cl introduced and the active centers. The whole reaction process is completed in the fluidized bed reactor. Thus, operating conditions and the structural design in the fluidized bed are closely related to the production efficiency of organosilicon monomers. The structural design of the distributor, as a key component of the fluidized bed reactor, directly affects the bubble motion characteristics and hydrodynamic behavior in bubble formation region, and further affects the heat and mass transfer in the bed [6-8]. In recent years, a host of experimental methods have been applied to investigate the effect of the distribution plate on gas-solid flow. Cooke et al. [9] conducted an experimental study of dry distillation of coal in a large-scale pilot plant with a diameter of 1.2 m. They found that about 50-90% of the reactions occur in the region 0.5 m above the distribution plate. Karri et al. [10] implemented an experiment to probe the penetration depth of the distribution plate, and concluded that the jet heights varied by up to 30% for fluid jets in different directions. Johnston et al. [11] experimentally investigated the flow state of the solid phase in the inlet zone of three different distributors. They pointed out that flow development length is extended by the superficial gas velocity. Knowlton et al. [12] determined that the pressure drop ratio of the distributor (K) for a porous or hood-shaped distributor is a constant. And the value of K is 0.3 for distributors with openings direction of the vertical or lateral while the value of K is 0.1 for distributors with opening downward. Zhang et al. [13] experimentally explored the effect of different distributor structures on the flow distribution of plate-fin heat exchangers and proposed a distributor structure with a fluid replenishment chamber.

With the development of the algorithms and processing power,

---

†To whom correspondence should be addressed.
E-mail: lvguoqiang_ok@aliyun.com

the use of two-fluid model based on the Euler-Euler approach (TFM) to simulate the complex reactions and gas-solid fluidization behavior in fluidized beds is becoming widespread, especially in the large-scale gas-solid fluidization systems [14-16]. Gas and solid phases are described as a continuum by TFM, and the drag force becomes the basis of the gas-solid coupling. The particle motion in gas-solid flow, including the airflow carries and transports particles, is determined by the magnitude of the drag force. Lu et al. [17] performed a simulation investigation of the behavior of bubbles and particles in a bubbling fluidized bed with a tubular distributor via Gidaspow drag model, and analyzed the effect of gas injection velocity and tubular distributor spacing on the fluidization state. They demonstrated that the optimal pipe spacing was 1.5-1.75 mm. Muhamad et al. [18] studied the effect of a 3-hole orifice plate on the fluidization state in a bubble bed lift tube using the Gidaspow drag model and found that the process of bubble formation, aggregation, and rupture was clearly described. Dong et al. [19] explored the effect of distributor perforated ratio on fluidization quality applying the Syamlal-O'Brien drag model, and the results showed that the root mean square (RMS) of bed pressure drop for the perforated ratio 0.46% of distributor was greater than that of the distributors with perforated ratio of 0.86% or 1.1%, and a larger discrepancy occurred as the perforated ratio of distributor was 0.46%. Son et al. [20] evaluated distributors of uniformity-type and nozzle-type via the Syamlal-O'Brien drag model. They proved that the two types of distributors exhibited similar behavior in terms of bed pressure drop along the axial height. Zhang et al. [21] designed two types distributors for Fischer-Tropsch synthesis and simulated the effect of two distributors on target product selectivity using the Syamlal-O'Brien drag model. They found that a higher conversion of small-diameter particles was obtained using the circular distributor in comparison with the branched pipe distributor under the same conditions.

Drag force is a vital parameter to characterize the momentum exchange and interaction between the gas-solid phases. Gas-solid drag force model was closely related to the accuracy of numerical simulation, and it can precisely simulate the particle velocity field in the two-fluid model. Gidaspow et al. [22,23] summarized the drag coefficients of Wen-Yu model and Ergun model under different solid phase fractions and proposed a drag model appropriate for the entire range of solid phase fractions. Lu et al. [24] proposed a new correction method for the continuity of the Gidaspow model. In this study, the optimization method of Syamlal-O'Brien drag model from Richardson-Zaki [25] type velocity-voidage correlation is incorporated in the CFD simulation by user-defined function (UDF). Several drag models in dense gas-solid flow, including the Wen-Yu drag model, the Gidaspow drag model, the Syamlal-O'Brien drag model and optimized drag model, were compared. The results show that optimized drag model can reasonably predict the gas-solid fluidization behavior of the organosilicon synthesis process. Meanwhile, from the perspective of gas-solid phase distribution, pressure fluctuation, bubble behavior, the performance of the distributor is analyzed based on the engineering design theory of the distributor, experimental data and numerical simulation, and a suitable distributor design method for silicone synthesis is proposed.

NUMERICAL MODEL AND METHODOLOGY

1. Numerical Model

A two-fluid model based on the Euler-Euler approach is used to increase the adaptability of the grid by averaging the differential equations for local and instantaneous behavior. Compared to the description of particle size in the Euler-Lagrange model, the model used here is based on the assumption of particle continuity at the macro scale. Thus, the equations for the particle and gas phases have the same form, which reduces the calculation time.

Based on the assumption of particle continuity, the particles and fluids are considered as continuous fluids that permeate each other.

$$\sum_{q=1}^{2}\alpha_q=1 \tag{1}$$

The continuity equation for phase q can be expressed as:

$$\frac{\partial}{\partial t}(\alpha_q\rho_q)+\nabla\cdot(\alpha_q\rho_q\vec{v}_q)=0 \tag{2}$$

The momentum conservation equation of the fluid phase can be given:

$$\begin{aligned}\frac{\partial}{\partial t}(\alpha_q\rho_q\vec{v}_q)+\nabla\cdot(\alpha_q\rho_q\vec{v}_q\vec{v}_q)&=-\alpha_q\nabla p+\nabla\cdot\bar{\bar{\tau}}_q+\alpha_q\rho_q\vec{g}\\&+\alpha_q\rho_q(\vec{F}_q+\vec{F}_{lift,\,q}+\vec{F}_{Vm,\,q})+\sum_{p=1}^{n}(K_{pq}(\vec{v}_p-\vec{v}_q)+\dot{m}_{pq}\vec{v}_{pq})\end{aligned} \tag{3}$$

where ρ_q represent the density of the fluid phase. $\vec{g}$, $\vec{F}_q$, $\vec{F}_{Vm,\,q}$ and $\vec{F}_{lift,\,q}$ stand for the acceleration of gravity, the external body force and virtual mass force of the q phase, respectively. $\vec{F}_{lift,\,q}$ is a lift force. K_{pq} is the interphase momentum exchange coefficient.

The momentum conservation equation of the solid phase is described as:

$$\begin{aligned}\frac{\partial}{\partial t}(\alpha_s\rho_s\vec{v}_s)+\nabla\cdot(\alpha_s\rho_s\vec{v}_s\vec{v}_s)&=-\alpha_s\nabla p+\nabla\cdot\bar{\bar{\tau}}_{s,\,0}+\alpha_s\rho_s\vec{g}\\&+\alpha_s\rho_s(\vec{F}_s+\vec{F}_{lift,\,s}+\vec{F}_{Vm,\,s})+\sum_{p=1}^{n}(K_{gs}(\vec{v}_g-\vec{v}_s)+\dot{m}_{gs}\vec{v}_{gs})\end{aligned} \tag{4}$$

where K_{gs} is the momentum exchange coefficient between fluid and solid phase. $\bar{\bar{\tau}}_{s,\,0}$ represents a pressure-strain tensor as follows:

$$\bar{\bar{\tau}}_{s,\,0}=\alpha_s\mu_s(\nabla\cdot v_s+\nabla\cdot v_s^T)+\alpha_s\left(\lambda_s-\frac{2}{3}\mu_s\right)\nabla\cdot v_s\bar{\bar{I}} \tag{5}$$

here μ_s and λ_s stand for, respectively, the shear and bulk viscosity of the solid phase.

Interphase resistance is the main interaction force between particles and fluid phase. The drag model widely used is summarized as follows:

(1) Syamlal-O'Brien drag model [26]

$$K_{gs}=\frac{3}{4}\frac{\rho_g\alpha_g\alpha_s}{v_{r,\,s}^2 d_s}C_D\left(\frac{Re}{v_r}\right)|\vec{v}_s-\vec{v}_g| \tag{6}$$

$$C_D=\left[0.63+\frac{4.8}{\sqrt{\frac{Re}{v_r}}}\right] \tag{7}$$

$$v_r=\frac{1}{2}[A-0.06Re+\sqrt{(0.06Re)^2+0.12Re(2B-A)+A^2}] \tag{8}$$

$$A=\alpha_g^{4.14} \tag{9}$$

$$B=\begin{cases} 0.8\alpha_g^{1.28}, & \alpha_g<0.85 \\ \alpha_g^{2.65}, & \alpha_g\geq 0.85 \end{cases} \tag{10}$$

where C_D is the drag coefficient. A and B are the constant in Syamlal-O'Brien drag model, respectively. v_r denotes terminal velocity coefficient of solid phase. Re stands for the particle Reynolds number.

(2) Correction method

$$C_D(Re, \varepsilon)=\frac{C_{D,s}(Re/v_{r,s})}{v_{r,s}^2} \tag{11}$$

where $C_D(Re, \varepsilon)$ represents the drag coefficient of a multi-particle. $C_{D,s}(Re, \varepsilon)$ is the drag coefficient of a single-particle, Ar denote the Archimedes number. The equation is described by:

$$\frac{v_{r,s}-A}{B-v_{r,s}}=0.06Re_s \tag{12}$$

$$Re_s=\frac{\sqrt{4.8^2+2.52\sqrt{\frac{4Ar}{3}}}-4.8}{1.26} \tag{13}$$

$$Ar=\frac{(\rho_s-\rho_g)d_s^3\rho_g g}{\mu_g^2} \tag{14}$$

$$A=\alpha_g^{4.14} \tag{15}$$

$$B=C_2\alpha_g^{1.28} \tag{16}$$

$$C_1=1.28+\frac{\log(C_2)}{\log(0.85)} \tag{17}$$

(3) Wen-Yu drag model [27]

$$K_{gs}=\frac{3\rho_g\alpha_g\alpha_s}{4d_s}C_D|\vec{v}_s-\vec{v}_g|\alpha_g^{-2.65} \tag{18}$$

$$C_D=\frac{24}{\alpha_g Re_s}[1+0.15(\alpha_g Re_s)^{0.687}] \tag{19}$$

$$Re_s=\frac{\rho_g d_s|\vec{v}_s-\vec{v}_g|}{\mu_g} \tag{20}$$

(4) Gidaspow drag model [28]

When $\alpha_g\geq 0.85$, K_{gs} can be obtained by Wen-Yu model, namely, Eq. (18) and Eq. (19).

When $\alpha_g<0.85$, K_{gs} can be obtained by Ergun equation as follows:

$$K_{gs}=150\frac{\alpha_g(1-\alpha_g)\mu_g}{\alpha_g d_s^2}+1.75\frac{\rho_g\alpha_s|\vec{v}_s-\vec{v}_g|}{d_s} \tag{21}$$

The solid pressure was used to calculate the pressure gradient term in the particle phase momentum equation in the compressible fluid. Due to the collisions between particles, the solid pressure consists of a kinetic energy term and a second term.

$$p_s=\alpha_g\alpha_s\Theta_s+2\rho_s(1+e_{s,s})\alpha_s^2 g_{R,ss}\Theta_s \tag{22}$$

where $e_{s,s}$ is the coefficient of restitution for particle collisions. $g_{R,ss}$ represents a radial distribution coefficient to modify the collision probability between particles. For the existence of one or more solid phases, the expression [29] is:

$$g_{R,ss}=\left[1-\left(\frac{\alpha_s}{\alpha_{s,max}}\right)^{\frac{1}{3}}\right]^{-1} \tag{23}$$

The kinetic energy conservation of moving particles is represented by particle temperature. According to the particle kinetic energy theory, the temperature of solid particles is proportional to the kinetic energy of particle motion. The transport equation can be written:

$$\frac{3}{2}\left[\frac{\partial}{\partial t}(\alpha_s\rho_s\Theta)+\nabla\cdot(\alpha_s\rho_s v_s\Theta_s)\right]=(-p_s\bar{\bar{I}}+\bar{\bar{\tau}}_s):\nabla v_s+\nabla\cdot(k_{\Theta_s}\nabla\Theta_s)-\gamma\Theta_s+\varphi_{gs} \tag{24}$$

The formula: $(-p_s\bar{\bar{I}}+\bar{\bar{\tau}}_s):\nabla v_s$ is energy generated by the solid tensor. $k_{\Theta_s}\nabla\Theta_s$ represents the energy diffusion. $\gamma\Theta_s$ stands for collision dissipation of energy.

2. Simulation Methodology

The three-dimensional geometrical model is performed on an MC synthesis, which is taken from experimental exploration of Zhang et al. [30,31]. In addition, the experiment investigates the critical fluidization velocity by the bed pressure drop method, and the bed pressure drop by the differential pressure sensor can be obtained. The PC6M device is utilized to measure the solid volume fraction distribution at 0.05 m above the gas distribution plate. A detailed description of the experiment can be observed in the literature [30,31]. A schematic of the model is illustrated in Fig. 1. The system consists of a 0.005 m pre-distributor, a 0.3 m bed reactor and a 0.003 m gas distributor. Initially, the fluidized bed is filled with a packed bed of silica particles with a diameter of 0.2 m. The computational domain is divided into three areas: the pre-distribution region, the distribution region, and the reaction region. Due

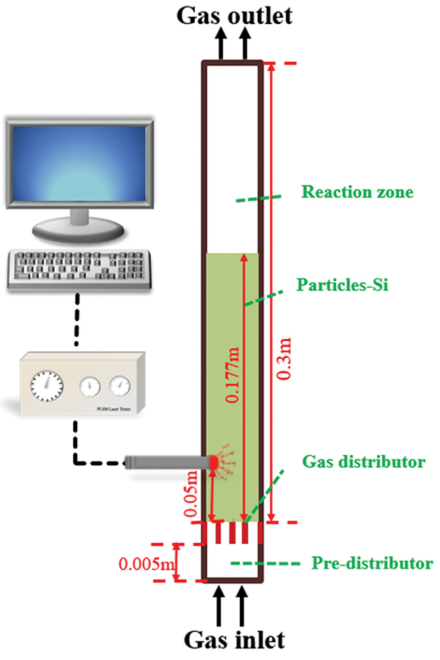

Fig. 1. Fluidized bed reactor.

Table 1. Geometry dimension of three types of distributors

Distributor perforated ratio (%)	Number of perforations	Distance between perforations (mm)	Diameter of perforations (mm)	Number of perforations in diameter
0.251	9	7	0.434	3
0.53	19	5	0.434	5
1	36	3.5	0.434	7

Table 2. Specific simulation parameters and material properties

Parameters	Value/comment
Geometry	
Width (m)	0.026
Height (m)	0.308
Static bed height (m)	0.177
Boundary condition	
Inlet type	Velocity-inlet
Outlet type	Pressure-outlet
Walls type	No slip
Initial conditions	
Superficial gas velocity (m/s)	1.56×10^{-2}
Operation velocity (m/s)	0-0.1
Initial solid packing	0.49
Particle	
Type	Si
Mean diameter (m)	2×10^{-4}
Density (kg/m^3)	2328.3
Restitution coefficient	0.9
Angle of internal friction	30
Gas	
Type	CH_3Cl
Density (kg/m^3)	2.22
Viscosity (Pa·s)	2.15×10^{-5}

to the large difference in geometric scale between the distributor aperture and the bed diameter, the distributor grid, a hexahedral mesh with a size of 0.0002 m×0.0002 m, is locally encrypted to improve the simulation accuracy and then reduce the runtime. To clearly observe the effect of the opening rate on the fluidization state, the opening rates are divided into three categories under optimal conditions, as shown in Table 1. Detailed information regarding the operation of specific parameters and material properties can be seen in Table 2. The three different open-aperture distribution plates are performed via commercial numerical simulation software of Fluent to predict the impact of opening rates on bubble behavior, bed pressure drop, and fluidization.

RESULTS AND DISCUSSION

1. Selection and Validation of Drag Model

The critical fluidization velocity is given by the following empirical formula [32]:

$$U_{mf}=\frac{9.0\times10^{-4}d_p^{1.8}[(\rho_p-\rho_f)g]^{0.94}}{\mu_f^{0.87}\rho_f^{0.066}} \tag{25}$$

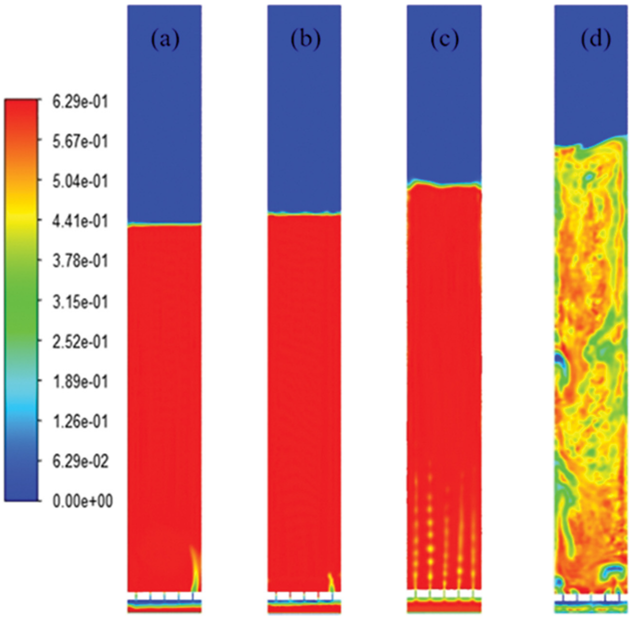

Fig. 2. Cloud plot of volume fraction distribution along the axial direction for different drag models with Φ=0.53% ((a) Syamlal-O'Brien, (b) Wen-Yu, (c) Gidaspow, (d) Modification).

The critical fluidization velocity is measured by Wu et al. It is basically consistent with the value calculated from Eq. (25). The experimental results show that the silicon conversion rate is highest, as the apparent gas velocity was 1.1 times the critical fluidization velocity. Therefore, the apparent velocity was set to 1.56×10^{-2} m/s in the simulations.

Currently, the interaction between particle phase and fluid phase mainly adopts the following drag model: Wen-Yu drag model, Gidaspow drag model and Syamlal-O'Brien drag model. The above drag model is evaluated on the distribution plate with opening area ratio of Φ=0.53%, n=19. The results show that a relatively stable state in the bed is reached at the simulation time of 9 s. And the axial section is unrelated to time at the simulation time larger than 9 s. Therefore, under different drag forces, the axial interface diagram of solid volume fraction at 12 s is shown in Fig. 2.

The method of drag force calculation has a significant impact on the accuracy of the two-fluid model simulation. Fig. 3 shows the curves of solid axial velocity at 0.05 m above the gas distribution plate under different drag models. According to previous research, it can be known that the three drag models of Syamlal-O'Brien, Gidaspow and Wen-Yu are empirical formulas summarized from experimental data of particle settling. Therefore, the three drag models exhibit the same distribution results. The results show that when the superficial gas velocity is 1.1 times the fluidization veloc-

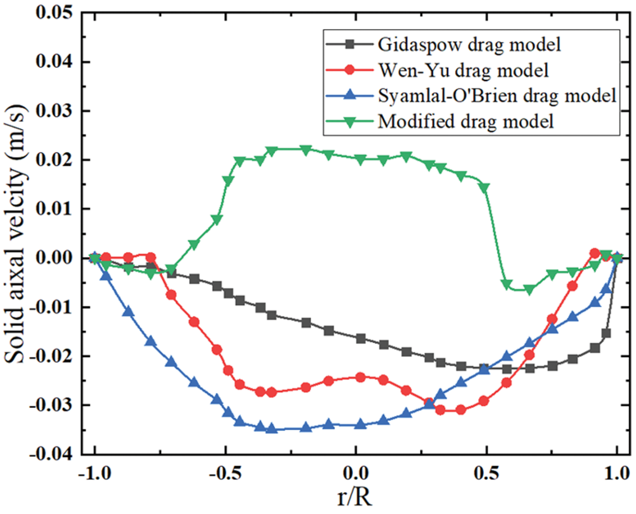

Fig. 3. The distribution of solid axial velocity in different drag models.

ity, the axial velocities of the particles are negative under the action of the three drag models and decreased from the wall to the center in the radial direction, indicating that the particles in the bed are not fluidized. Hence, it is clear that the three drag models underestimate the interactions between the particle and fluid phases. But there are also clear differences between them. Gidaspow uses the Ergun equation to solve the disadvantage that Wen-Yu was only suitable for dilute phase gas-solid systems, but the pressure drop data used by Ergun is based on a packed bed with a solid holdup of 0.4-0.6, which leads, in this case, to a larger interphase force for Gidaspow than for Syamlal-O'Brien. Although Syamlal-O'Brien solved the discontinuity problem of Gidaspow at solid fraction at 0.8, and it was better than Ergun's formula at solid holdup at 0.5-0.6. However, the influence of particle shape and particle size configuration is not considered in the derivation of general empirical drag relationship. In this work, Reylows' and Archimedes' criterion numbers are introduced and to modify the original drag law and modify the original drag law and include commonly used experimental properties for specific materials. The detailed method is described in Eqs. (11)-(17). Fig. 3 shows that using the modified drag model results in significantly different axial velocity curves for the solids, and that most of the data points are positive, indicating that most of the particles in the bed are fluidized. Fig. 4 shows that when the height from the distribution plate is 0.05 m, the calculated solid volume fractions are in good agreement with the test data of Zhang, and the simulation error is less than 3%. Indicating that the optimized drag model can accurately predict the behavior of the gas-solid phase.

2. The Effect of Opening Rate on Gas-Solid Fluidization Characteristics

It is necessary to keep the bed stable while minimizing the pressure drop in designing the distributor opening rate. The critical pressure drop of the distributor, $(\Delta p_D)_{CP}$, is calculated as:

$$(\Delta p_D)_{CP}=R_{CP}\times\Delta P_B \tag{26}$$

where R_{CP} is critical pressure drop ratio of distributor, and ΔP_B represents the bed pressure drop.

Qureshi et al. [33] proposed a correlation for calculating the critical pressure drop ratio, R_{CP}, which can be expressed as:

$$R_{CP}=0.01+0.2\left[1-\exp\left(\frac{0.5D_B}{L_B}\right)\right] \tag{27}$$

D_B and L_B stand for, respectively, the diameter and the height of the fluidized bed.

The perforated ratio of the distributor, α, is as follows:

$$\alpha=\left(\frac{\xi_D U^2\rho_f}{2g(\Delta p_D)_{DP}}\right) \tag{28}$$

where ξ_D(=2.0) is the resistance coefficient of distributor. U represents superficial velocity of bed near distributor.

The opening rate has a direct impact on the fluidization characteristics of the bed. In this study, the opening rate is improved by increasing the number of openings on the basis of same pore size. According to Eqs. (26)-(28), three groups of different opening ratios

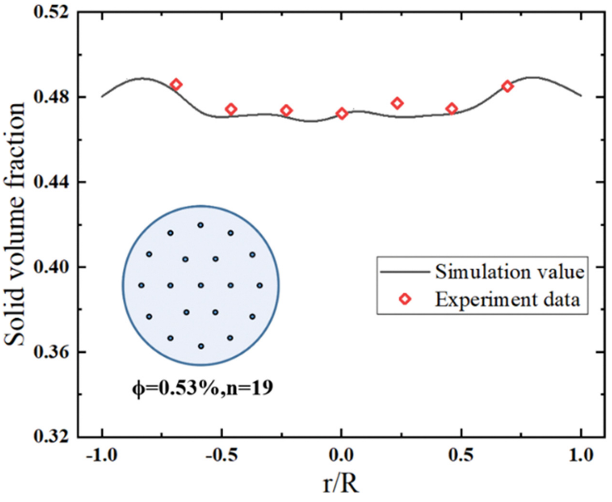

Fig. 4. Comparison of solid volume fraction Curve between simulation and experiment at Φ=0.53%, n=19.

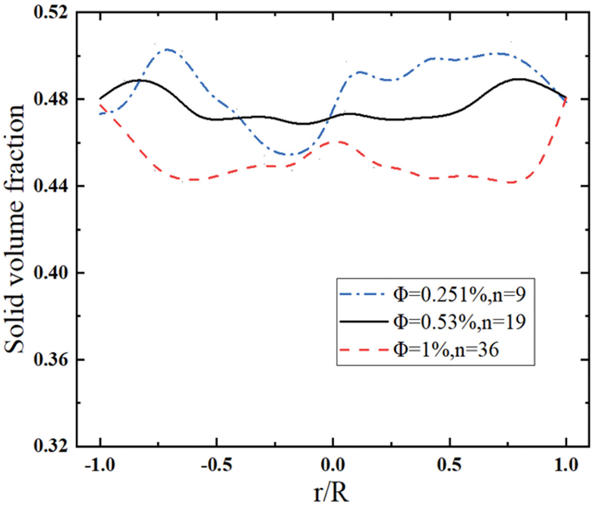

Fig. 5. Curves of solid volume fraction at different opening ratios.

are selected for simulation comparison, as shown in Table 1. Fig. 5 shows the solid volume fraction distributions under the different opening rates at a height of 0.05 m from the gas distribution plate. The results show that, as the superficial gas velocity is only 1.1 times the critical fluidization velocity, the solid volume fraction of the fluidized bed is uniformly distributed along the axial direction and does not change significantly with time. When Φ increases to 1% under the same superficial gas velocity, both the resistance of the distribution plate and the pressure drop of the critical empty tower decrease, resulting in a higher superficial gas velocity in the bed, and the solid volume fraction decreases compared to the first two opening rates. When Φ=0.53%, however, the fluctuation frequency and amplitude of the solid volume fraction are lowest, indicating an improved fluidization state and better heat and mass transfer inside the bed, which may be due to the change in the pressure drop of the distributor caused by changing the opening rate. This claim was also supported by Lim et al. in their report [34].

3. Relationship Between Opening Ratio and Distributor Pressure Drop

In view of the results from section 3.2, the pressure drop in three distribution plates is explored with the difference of opening rate and flow velocity. The curves of pressure drop can be seen in Fig. 6. At designing the distributor, the pressure drop, Δp_D, can be expressed in terms of the apparent velocity of the near bed the distributor. The equation can be described, as follows:

$$\Delta p_D = \xi_D \frac{U^2 \rho_f}{2\alpha^2 g} \tag{29}$$

To make the fluid flow through the distributor and into the reactor bed more uniform, the distributor must have a certain resistance. Fig. 6 shows the pressure drop curves at different flow velocities of three distribution plates with different opening rates. The results show that the opening rate has a significant influence on the pressure drop of the distribution plate. As the bed porosity increases, the resistance of the fluid flowing through the distribution plate decreases, ascribed to the pressure drop to decrease. So, the distribution plate can pass more fluid through the bed under the condition that other operating parameters remain unchanged, but it is not the larger the opening rate, the better. The pressure drop of distribution plate has a large difference as the opening rates of the porous plate are 0.53% and 1%, indicating that the pressure drop of the distributor rapidly decreases as the opening rate is larger than 0.53%, and resulting in non-uniform distribution of particles near the distributor. Further, when the opening rate is constant, the apparent gas velocity is the main factor affecting the pressure drop of the distribution plate. Enhancing the flow rate increases resistance and then enlarges the pressure drop. The pressure drop is obviously augmented as the flow rate is larger than 0.08 m/s.

4. Relationship Between Bed Height and Bed Pressure Drop

ΔP_B, the theoretical pressure drop of the bed, is given by:

$$\Delta P_B = [\rho_s(1-\varepsilon_{mf}) + \rho_f \varepsilon_{mf}]gH \tag{30}$$

The value of ΔP_B calculated via Eq. (32) is 2,399 Pa, and the average pressure drop in the numerical simulation is 2,105 Pa, which is consistent with the theoretical value. Additionally, the initial pressure drop measured by the differential pressure sensor is 1,940 Pa, which increased to 2,340 Pa at t=420 min. Fig. 7 illustrates the pressure drop curves along the height of the bed under the different distributors. The tested pressure drop result is consistent with the simulated data. However, the pressure drop varies with the opening rate, demonstrating that the bed pressure drop is impacted via design parameters of fluidized bed. Eq. (29) shows that ΔP_D is negatively correlated with the porosity. In the engineering design of the distributor, the $\Delta P_D/\Delta P_B$ ratio and the R is generally required to be between 0.7 and 0.14. Here, the R values of three different porosity distribution plates are 0.1458, 0.11679, and 0.078. respectively. The greater the value of R, the greater the resistance of gas flow through the distribution plate, and the particle distribution is more uniform at the initial moment. It indicates that the fluidization quality of the heat and mass transfer effect is strengthened. However, if the pressure drop of the distributor is too large, this will result in more wear on the catalyst particles and reaction particles. There-

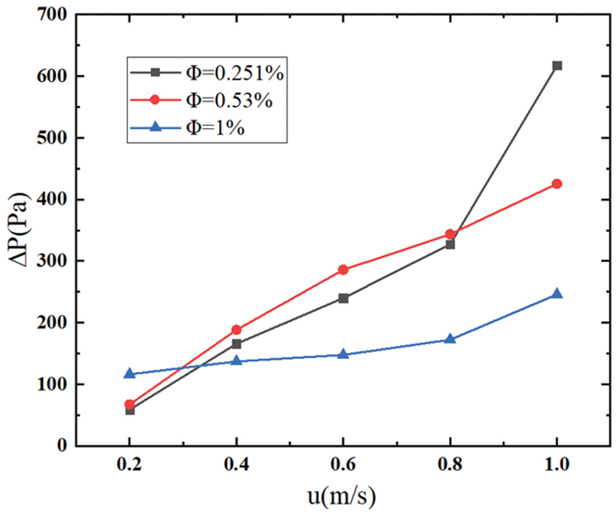

Fig. 6. Curves of pressure drop of three opening ratios at different flow velocities.

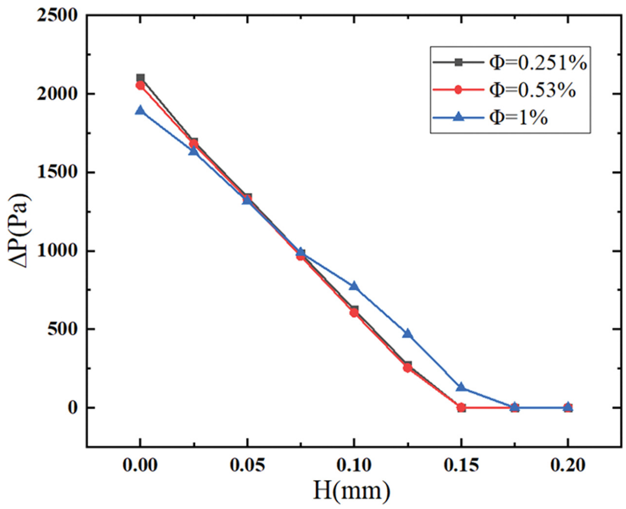

Fig. 7. Average pressure drop along the axial normal direction for three opening ratios.

fore, the R value should not be too large in designing the distributor. Hence, the distribution plate with an opening rate of 0.53% is deemed suitable for the system.

5. Relationship Between Bubble Behavior and Different Porosity and Gas Velocity

The area in the vicinity of the porous plate distributor has profound meaning for the periodic changes of the bubble distribution. Due to that intense disturbances exist between the particle and fluid phases, and then intensify the contacting efficiency between two phases. In particular, bubbles are the driving force for the circulation and backmixing of particles in the bed. So, the mass, momentum, and energy exchange in two phases are increased, and the heterogeneous chemical reaction is greatly promoted.

Mori and Wen proposed a method for calculating bubble size, [35] as follows:

$$D_P = D_{P,\infty} - (D_{P,\infty} - D_{P,0})\exp(-0.3H_B/D_B) \qquad (31)$$

where D_P represents the average bubble size when the bed height is H_B.

The maximum bubble size, $D_{P,\infty}$, can be expressed:

$$D_{P,\infty} = 1.49[D_B^2(u - u_{mf})]^{0.4} \qquad (32)$$

Its initial bubble size, $D_{P,0}$, can be expressed:

$$D_{P,0} = 1.38g^{-0.2}[A_B(u - u_{mf})]^{0.4} \qquad (33)$$

where A_B=s/n. D_B is the reactor diameter.

Fig. 8 shows the solid volume fraction distributions near the three different porous plate distributors as well as the streamlined diagram of CH_3Cl. Eq. (31)-(33) shows that the bubble size is negatively correlated with the opening rate, which is consistent with

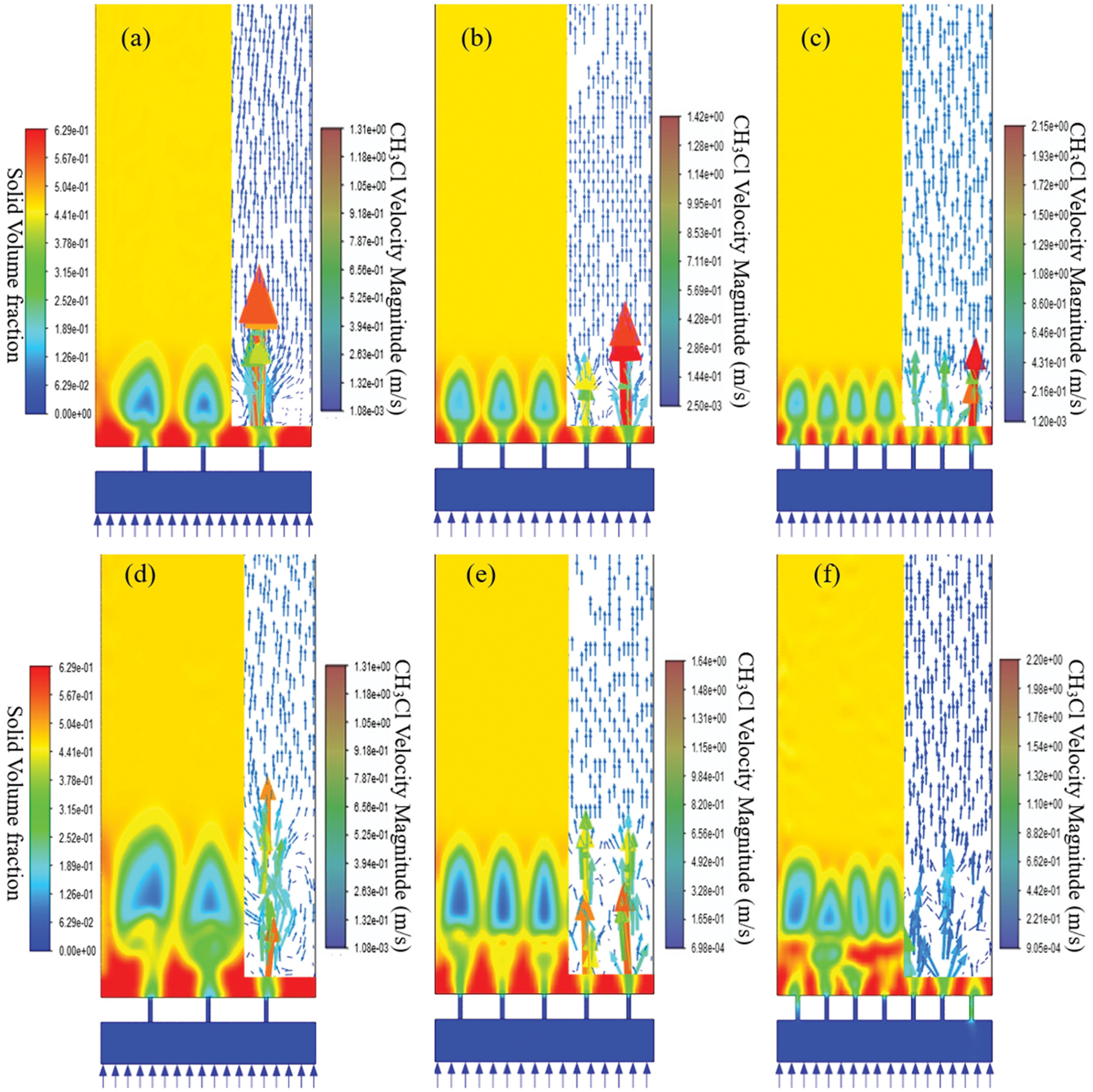

Fig. 8. Volume fraction distribution of solids with three different opening ratios and streamline of CH_3Cl.

the simulation results as shown in Fig. 8. As given in Fig. 8, bubbles gather near the distributor and move slowly towards the center of the reactor. After reaching the critical jet height, the particles are separated, then slowly move downward along the wall to form local circulation patterns. The initial bubble diameter and the height of the bubble formation zone are consistent with the experiment result of Tsukada et al. [36]. Further, the penetration depth decreases with the porosity increases. This is helpful for the particle size distribution in the bed. This phenomenon is ascribed to the fact that, the penetration depth with a higher will result in severe wear of particle of reaction and catalytic. That not only increases the cost of the process, but also affects the quality of fluidization. The change in jet depth is not obvious when the porosity increases to 0.53%. The resistance of the porous plate decreases with the opening rate increase in the opening rate, in consequence of more CH_3Cl gas passing through the bed in the form of bubbles, which enhances the jet velocity of the gas.

6. Effect of Pressure Pulsation on Bubble Behavior at Different Opening Rates

Pressure fluctuation is the comprehensive performance of particle fluidization quality in the bed. Bubble generation, aggregation, and fragmentation, as well as judging the fluidization characteristics of the bed, are described to the signal of pressure fluctuation. σ_B, the standard deviation of bed pressure, is proportional to the pressure fluctuation in the bed and the resistance of the particle phase.

$$\sigma_B=\sqrt{\frac{1}{N-1}\sum_{i=1}^{N}(p_i-\bar{p})^2} \qquad (34)$$

The pressure fluctuation curves in different opening rates along the axial height, calculated in Eq. (34), can be seen in Fig. 9 The formation of each bubble is accompanied by a large pressure fluctuation, and the changes of bubbles size will also affect the amplitude of pressure fluctuation. As given in Fig. 9, the distributor has more gas inlets with the opening ratio increases, causing the decrease of gas phase momentum loss Therefore, a larger opening ratio produces more bubbles at the onset of fluidization (and hence a larger σ_B). With the increase of the axial bed height, the transformation of the bubble aggregation and fragmentation behavior becomes more frequent during ascent with larger opening ratios and the up and down trend of the σ_B. Finally, once the bubble breaks through the bed interface and ruptures, σ_B tends to a steady value. Therefore, this analysis shows that the present simulation model can accurately predict the pressure fluctuation characteristics in the bed.

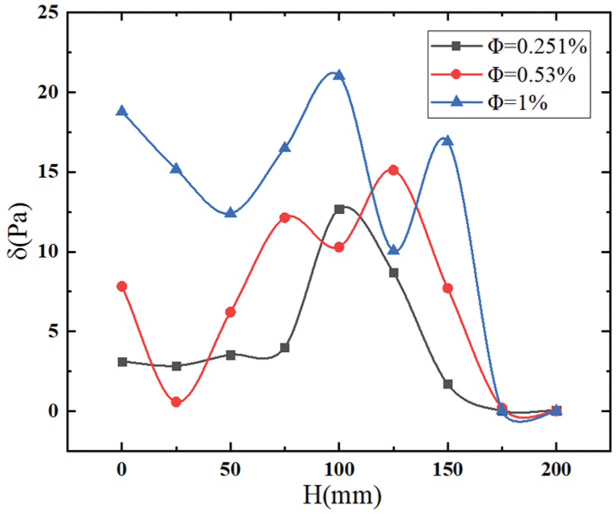

Fig. 9. Distribution of pressure fluctuation curve along axial height under three opening ratios.

7. Power Spectrum Analysis of Pressure Signal

The formation and movement of bubbles leads to the uneven structure of the bed, and the coalescence and fragmentation of the bubbles during the ascent process is the cause of the local pressure variation. The phenomenon has also been proved in Section 3.6, and Abed also confirmed this result [37]. Therefore, pressure fluctuations in the reactor become a sign of distribution inhomogeneity. The effect of heat and mass transfer is an objective manifestation of inhomogeneity. When the inhomogeneity is weakened, the heat and mass transfer effect will be enhanced. When the discrete time domain signals are transformed into frequency domain signals via Fourier transform, the frequency with the highest amplitude is called the principal frequency. In the case of a fluidized bed, the principal frequency of the pressure signal represents the frequency of bubble generation in the bed, and the magnitude of the pressure fluctuation represents the bubble size. Therefore, the presence of a higher frequency and a lower fluctuation amplitude implies the existence of small bubbles. It means that the inhomogeneity is weakened. As given in Fig. 10, the main frequencies at all three opening rates are less than 1 Hz, and values are 0.035 kPa,

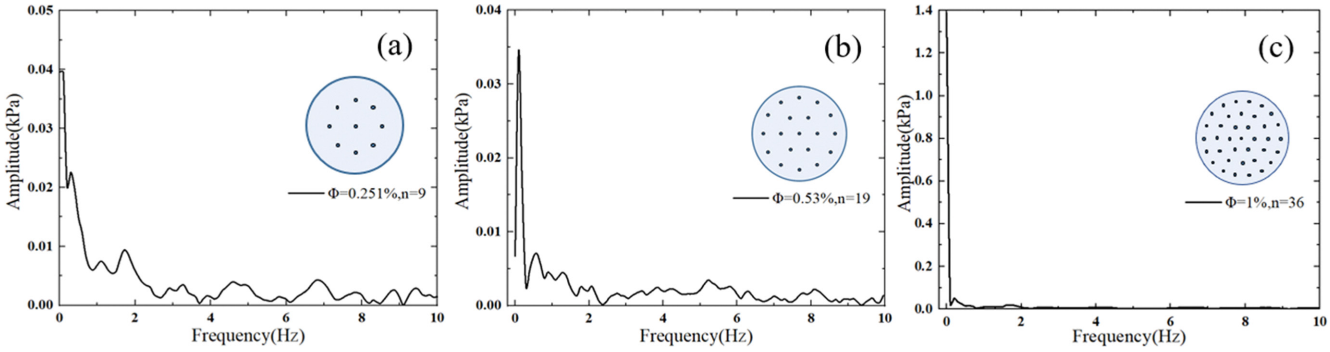

Fig. 10. Power spectrum analysis diagram under three opening rates.

0.04 kPa, and 1 kPa for opening rates of 0.53%, 0.251%, and 1%, respectively. This shows that the open porosity of 0.53% has both a high frequency and a low amplitude, which corresponds to favorable efficiency of heat and mass transfer.

CONCLUSIONS

A modified Syamlal-O'Brien drag force model based on Richardson-Zaki theory under the Euler-Euler framework was implemented using Ansys Fluent. A particle dynamics method was used to numerically simulate three different porosity distributors. The conclusions are as follows:

(1) The simulation results of the CFD software package Fluent are in accord with the experimental data. The error between simulation data and experimental data is less than 3%. The optimized drag model can accurately predict gas-solid fluidization behavior in the fluidized bed reactor.

(2) The opening ratio of distributor has a significant effect on the gas-solid distribution. At the opening ratio of 0.53%, the non-uniformity of solid fraction distribution is the lowest and the efficiency of heat and mass transfer in the bed is enhanced. In addition, this conclusion is also proved by pressure drop analysis, bubble behavior, pressure pulsation and power spectrum analysis.

(3) The resistance loss of different opening ratios was evaluated by the pressure drop ratio of the distributor. The results show that opening ratio of 0.53% can preferably meet the design criteria of reducing dissipation while increasing fluidization quality.

(4) This model clearly observes the instantaneous distribution of bubbles and proves that the bubble behavior is the main factor affecting the pressure pulsation. The results indicate that pressure fluctuation is the most acute at the bed height of 70-130 mm.

ACKNOWLEDGEMENT

Science and Technology Planning Project of Yunnan Science and Technology Department (No. 202002AB080002).

NOMENCLATURE

A : constant in Syamlal-O'Brien drag model [-]
Ar : the Archimedes number [-]
B : constant in Syamlal-O'Brien drag model [-]
C_D : drag coefficient [-]
D_B : diameter of solid particle [m]
$e_{s,s}$: restitution coefficient of solid phase [-]
$\vec{F}_q$: the external body force [N]
$\vec{F}_{Vm,q}$: the virtual mass force [N]
$\vec{F}_{lift,q}$: the lift force [N]
g : the gravitational acceleration $[m\cdot s^{-1}]$
$g_{0,ss}$: the general radial distribution function [-]
L_B : the height of fluidized bed [m]
$\bar{\bar{I}}$: the unit tensor [-]
K_{gs} : drag factor of phase solid in phase gas $[kg\cdot m^{-3}\cdot s^{-1}]$
n : number of holes
P : pressure [Pa]
P_s : solids pressure [Pa]
R_{CP} : the critical pressure drop ratio of distributor [-]
Re : the Reynolds number [-]
t : time [s]
U_{mf} : the critical fluidization $[m\cdot s^{-1}]$
U : the superficial velocity of bed near distributor $[m\cdot s^{-1}]$
α : volume fraction [-]
ρ : density $[kg\cdot m^{-3}]$
μ : shear viscosity $[kg\cdot m^{-1}\cdot s^{-1}]$
λ : bulk viscosity $[kg\cdot m^{-1}\cdot s^{-1}]$
ξ_D : the resistance coefficient of distributor [-]
Θ : granular temperature $[m^2\cdot s^{-2}]$
$v_{r,s}$: the relative velocity correlation [-]
$\bar{\bar{\tau}}_{s,0}$: the pressure strain tensor [Pa]
σ_B : the standard deviation of bed pressure [Pa]
Φ : opening area ratio

Subscripts

s : solid phase
q : fluid phase
t : terminal

NOTES

The authors declare no competing financial interest.

REFERENCES

1. E. Yilgör and I. Yilgör, *Prog. Polym. Sci.*, **39**(6), 1165 (2014).
2. G. Maier, J. Glatthaar and H. P. Reisenauer, *J. Organomet. Chem.*, **686**(1), 341 (2003).
3. Y. Zhang, Y. Ji, J. Li, H. Liu, Z. Zhong and F. Su, *J. Catal.*, **348**, 233 (2017).
4. D. T. Hurd and E. G. Rochow, *J. Am. Chem. Soc.*, **67**(7), 1057 (1945).
5. E. G. Rochow, *J. Am. Chem. Soc.*, **67**(6), 383 (1964).
6. M. Polli, M. D. Stanislao, R. Bagatin, E. A. Bakr and M. Masi, *Chem. Eng. Sci.*, **57**(1), 197 (2002).
7. X. B. Qi, W. X. Huang and J. Zhu, *Chem. Eng. Technol.*, **31**(4), 542 (2008).
8. Q. Guo, J. Werther, C. Aue-Klett and E. Hartge, *AIChE J.*, **51**(5), 1359 (2005).
9. M. J. Cooke and W. Harris, *Tripartite chemical engineering conference symposium on fluidization*, Montreel (1968).
10. S. B. R. Karri, *PSR1 Research Report No. 60*, (5), 235 (1990).
11. P. M. Johnston, J. Zhu, H. I. de Lasa and H. Zhang, *AIChE J.*, **45**(7), 1587 (1999).
12. S. Karri and T. M. Knowlton, *Gas distributor and plenum design in fluidized beds*, Fluidization Solids Handling & Processing (1999).
13. Z. Zhang, Y. Li and Q. Xu, *Heat Transfer-Asian Res.*, **33**(6), 402 (2004).
14. S. Wang, K. Luo and J. Fan, *Chem. Eng. Sci.*, **217**, 115550 (2020).
15. S. Wang, K. Luo, C. Hu, L. Sun and J. Fan, *Powder Technol.*, **333**, 304 (2018).
16. S. Yang, S. Wang and H. Wang, *Energ. Convers. Manage.*, **223**, 113439 (2020).

17. L. Huilin, Z. Yunhua, J. Ding, Z. Linyan and L. Yaning, *Ind. Eng. Chem. Res.*, **45**(20), 6818 (2006).
18. M. H. B. Ibrahim, N. K. M. Najib and S. Karuppanan, *AIP Conference Proceedings*, **1482**, 69 (2012).
19. S. Dong, C. Cao, C. Si and Q. Guo, *Ind. Eng. Chem. Res.*, **48**(1), 517 (2009).
20. S. I. Ngo, Y. Lim, B. Song, U. Lee, J. Lee and J. Song, *Powder Technol.*, **275**, 188 (2015).
21. X. Zhang, G. Zhai, W. Qian, H. Zhang, Q. Sun and W. Ying, *Particuology*, **45**, 98 (2019).
22. J. Ding and D. Gidaspow, *AIChE J.*, **36**(4), 523 (1990).
23. D. Gidaspow, J. Jung and R. K. Singh, *Powder Technol.*, **148**(2-3), 123 (2004).
24. L. Huilin and D. Gidaspow, *Chem. Eng. Sci.*, **58**(16), 3777 (2003).
25. M. Syamlal and T. J. O'Brien, *The derivation of a drag coefficient formula from velocity-voidage correlations*, US Department of Energy, Morgantown (1987).
26. M. Syamlal and T. J. O'Brien, *Int. J. Multiphas. Flow.*, **14**(4), 473 (1988).
27. C. Y. Wen and Y. H. Yu, *Chem. Eng. Prog., Symp. Ser.*, **61**(1), 100 (1966).
28. L. Huilin and D. Gidaspow, *Chem. Eng. Sci.*, **58**(16), 3777 (2003).
29. S. Zimmermann and F. Taghipour, *Ind. Eng. Chem. Res.*, **44**(26), 9818 (2005).
30. F. Zhang, Z. Zhang, Y. Liu, Z. Zhong and W. Xing, *Ind. Eng. Chem. Res.*, **55**(40), 10600 (2016).
31. J. Wu, W. Xing, F. Zhang, Z. Zhong, W. Jin and N. Xu, *CIESC J.*, **65**(07), 2776 (2014).
32. A. R. Abrahamsen and D. Geldart, *Powder Technol.*, **26**(1), 35 (1980).
33. A. E. Qureshi and D. E. Creasy, *Powder Technol.*, **22**(1), 113 (1979).
34. J. H. Lim, Y. Lee, J. H. Shin, K. Bae, J. H. Han and D. H. Lee, *Powder Technol.*, **266**, 312 (2014).
35. S. Mori and C. Y. Wen, *AIChE J.*, **21**(1), 109 (1975).
36. M. Tsukada and M. Horio, *Powder Technol.*, **60**(1), 69 (1990).
37. R. Abed, *Ind. Eng. Chem. Fundam.*, **24**(1), 78 (1985).